Holographic superfluid flows with a localized repulsive potential

Akihiro Ishibashi,[1,*] Kengo Maeda,[2,†] and Takashi Okamura[3,‡]

[1] *Department of Physics, Kindai University, Higashi-Osaka 577-8502, JAPAN*
[2] *Faculty of Engineering, Shibaura Institute of Technology, Saitama 330-8570, JAPAN*
[3] *Department of Physics, Kwansei Gakuin University, Sanda, Hyogo, 669-1337, JAPAN*

We investigate a holographic model of superfluid flows with an external repulsive potential. When the strength of the potential is sufficiently weak, we analytically construct two steady superfluid flow solutions. As the strength of the potential is increased, the two solutions merge into a single critical solution at a critical strength, and then disappear above the critical value, as predicted by a saddle-node bifurcation theory. We also analyze the spectral function of fluctuations around the solutions under a certain decoupling approximation.

arXiv:1606.04668v1 [hep-th] 15 Jun 2016

I. INTRODUCTION

Superfluid flow in Bose-Einstein condensate in cold atoms or in ^{4}He is of particular interest as an example of inviscid fluid flows with no dissipation. It is typically unstable due to the excitation of the flow (the Landau instability) or against the creation of solitons such as vortices (the soliton-emission instability). In particular, the latter instability is expected to occur in spatially inhomogeneous systems or around an obstacle [1].

The soliton-emission instability in inhomogeneous systems has been extensively investigated by solving the time-dependent Gross-Pitaevskii (GP) equation [2, 3]. Frisch et. al. [4] numerically found a steady superfluid flow solution in a two-dimensional system and showed that the flow is broken by the creation of vortices beyond a threshold velocity. Hakim [5] obtained two analytic steady superfluid flow solutions in one-dimensional system in the presence of an external localized repulsive potential. They merge at a critical velocity, and beyond it, there is no steady flow solution. These features are consistent with experimental results [6–8], and they can be described in terms of a saddle-node bifurcation of the stationary solutions [9]. However we should note that although the GP equation is very useful to understand various features of superfluid flows, it is applicable only to weakly interacting low temperature systems.

One of the possible approaches to tackling strongly interacting cases is to appeal to a "holographic model" based on the AdS/CFT duality [10]. There have already been a number of works on holographic models [11, 12] in which strongly correlated condensed matter systems can be successfully described in terms of some gravitational theory via the AdS/CFT duality (see also Ref. [13] for a review).

In this paper, we shall construct a holographic superfluid model as an attempt to extend the analysis of the one-dimensional superfluid flow in [5] to the strongly coupled case. We perturbatively construct analytic superfluid flow solutions (see also [14, 15] for similar flow solutions) in the presence of an external localized repulsive potential. We find that two steady flow solutions exist below a critical value of the strength of the potential. One of the solutions is unstable and steeper near the potential than the stable one, as shown in [5]. The two solutions merge into one at the critical value and then disappear beyond it, as predicted by a saddle-node bifurcation theory.

We also derive the spectral function ρ of fluctuations of the solution and investigate the effects of the impurity generated by the repulsive potential, under a certain decoupling approximation. We find that with respect to a small variation of the chemical potential, the spectral function shows a peculiar behavior which is explained by the existence of a band gap generated by the external localized repulsive potential.

This paper is organized as follows. In Sec. II, we set up our holographic model that corresponds to the one-dimensional superfluid flow studied in [5]. In Sec. III, we perturbatively construct two steady solutions of holographic superfluid flows and derive the superfluid current. In Sec. IV, we shall show that the steeper solution is unstable in the sense that the free energy is higher than that of the other solution. We study the spectral function in Sec. V. Sec. VI is devoted to summary and discussions.

II. HOLOGRAPHIC SUPERFLUID MODEL

We will construct a holographic superfluid model which is dual to a strongly coupled field theory in $3+1$-dimensional Minkowski spacetime with the action

$$S = \int d^5x\sqrt{-g}\left[R + \frac{12}{L^2} + \frac{L^2}{e^2}\mathcal{L}_m\right] + S_{\rm ct},$$
$$\mathcal{L}_m := -|D\psi|^2 - \left(m^2 + V(x,u)\right)|\psi|^2 - \frac{1}{4}F_{\mu\nu}F^{\mu\nu}\ , \quad (1)$$

where ψ is a complex scalar field with mass m and charge e, $D_\mu := \nabla_\mu - i\,A_\mu$, and where L denotes the AdS radius, $V(x,u)$ a localized external repulsive potential, and $S_{\rm ct}$ the counter term defined below.

*akihiro@phys.kindai.ac.jp
†maeda302@sic.shibaura-it.ac.jp
‡tokamura@kwansei.ac.jp

In this paper, we consider a probe limit $e \to \infty$ in which the gauge field A_μ and the scalar field ψ do not backreact on the original metric. Therefore we consider, as our background spacetime, the Schwarzschild-AdS metric with the temperature T:

$$\frac{ds^2}{L^2} = \frac{\pi^2 T^2}{u}\left(-f\,dt^2 + dx^2 + dy^2 + dz^2\right) + \frac{du^2}{4u^2 f}, \quad (2)$$

where $f(u) := 1 - u^2$, and $0 < u < 1$ outside the black hole with AdS boundary at $u = 0$.

The field equations on our background are

$$D^\mu D_\mu \psi - m^2\psi - V(x,u)\psi = 0\,, \quad (3)$$
$$\nabla_\nu F^{\nu\mu} = i[\psi^* D^\mu\psi - \psi(D^\mu\psi)^*]\,. \quad (4)$$

For simplicity, we shall set $m^2L^2 = -4$ so that the Breitenlohner-Freedman(BF) bound [16] is saturated, and consider a periodic potential with a dimensionless positive constant $\hat{g}$

$$V(x,u) = \frac{\hat{g}}{L}\,u \sum_{n=-\infty}^{\infty} \delta(x - nl)\,, \quad (5)$$

localized at $x_n = nl$ ($n \in \mathbb{N}$). Note that V corresponds to a repulsive potential, as $(\hat{g}/L)\,u$ is positive.

Since $V(x,u)$ decreases to zero as $u \to 0$ and thus the effective mass-squared saturates the BF bound at the AdS boundary, the asymptotic form of ψ becomes

$$\psi(u,x) \simeq -\alpha(x)u + \beta(x)u\ln u. \quad (6)$$

According to the dictionary of AdS/CFT duality, the coefficient α corresponds to the expectation value $\langle\mathcal{O}\rangle$ of the dual field theory operator of dimension two, while β corresponds to a source term in the dual boundary field theory [17]. Hereafter, we shall impose $\beta = 0$ at the AdS boundary, as our boundary condition on ψ.

As indicated in [14], it is convenient to use the following gauge invariant variables R and M_μ defined by $\psi = Re^{i\varphi}/L$ (where R is a dimensionless quantity) and $M_\mu := A_\mu - \nabla_\mu\varphi$. Then, Eqs. (3) and (4) reduce to the equations only for the gauge-invariant variables R and M_μ,

$$\nabla^2 R - M^\mu M_\mu R - m^2 R - V(x,u)R = 0\,, \quad (7)$$
$$\nabla^\mu(M_\mu R^2) = 0\,, \quad (8)$$
$$\nabla_\nu F^{\nu\mu} = \frac{2R^2}{L^2}M^\mu\,, \quad (9)$$

where Eqs. (7) and (8) are derived from the real and imaginary parts of Eq. (3), respectively. When the system is stationary, Eq. (8) implies the conservation of momentum of the superfluid flow.

According to the Bloch's theorem [18], having the periodic potential V, Eq. (3) must admit a solution ψ that is periodic in x, except the phase φ. This implies that for such a periodic solution ψ, the corresponding gauge invariants, R and M_μ, must also be periodic in x. So, hereafter we shall regard R and M_μ as smooth functions (apart from the location of the delta function in Eq. (5)) on an annulus $(u,x) \in [0,1]\times\mathbf{S}^1$ with $x = 0$ and $x = l$ being identified.

Since the potential is x-dependent, the velocity of the superfluid is also x-dependent. We consider the case that the superfluid velocity is injected at $x = l/2$ (compare with [5], in which the injection is made at spatial infinity). We impose the following asymptotic boundary conditions

$$M_t(0,x) = \mu\,, \qquad M_x(0,l/2) = v_0\,, \quad (10)$$

where μ and v_0 are respectively interpreted as the chemical potential and the superfluid velocity injected at $x = l/2$ (see, for example [19]).

III. PERTURBATIVE CONSTRUCTION OF THE SOLUTIONS, (R, M)

In this section we solve Eqs. (7), (8), and (9) perturbatively, assuming that the amplitude of R be very small. Following [20], we expand R and M_μ as a series in a small parameter ϵ as

$$\begin{aligned} R &= \epsilon^{\frac{1}{2}}R_1(u,x) + \epsilon^{\frac{3}{2}}R_2(u,x) + \cdots\,,\\ M_\mu &= M_\mu^{(0)}(u,x) + \epsilon M_\mu^{(1)}(u,x) + \cdots\,,\\ F_{\mu\nu} &= F_{\mu\nu}^{(0)} + \epsilon F_{\mu\nu}^{(1)} + \cdots\,, \end{aligned} \quad (11)$$

where $F_{\mu\nu}^{(i)} = \partial_\mu M_\nu^{(i)} - \partial_\nu M_\mu^{(i)}$.

At zeroth order in ϵ, imposing that the chemical potential $M_t^{(0)}(0,x)$ is constant, we find the solution for $M_\mu^{(0)}(u,x)$ as

$$M_t^{(0)} = \mu_0(1-u)\,, \quad M_x^{(0)} = \xi(x)\,, \quad M_u^{(0)} = 0\,. \quad (12)$$

Here, $\xi(x)$ is the velocity of the superfluid satisfying $\xi(l/2) = v_0$ (see the condition (10)).

Under the ansatz $R_1 = \rho(u)\zeta(x)$, Eq. (7) is divided into the following two equations:

$$\partial_x^2\zeta - \xi^2\zeta - g\delta(x)\zeta = -\kappa^2\zeta\,, \quad (13)$$
$$\rho'' - \frac{1+u^2}{u\,f}\rho' + \frac{1}{f}\left[\frac{1}{u^2} + \frac{\hat{\mu}_0^2\,(1-u)}{4u(1+u)} - \frac{\hat{\kappa}^2}{4u}\right]\rho = 0\,, \quad (14)$$

where $\kappa > 0$ is a separation constant, and where $g := \hat{g}L\,\pi^2\,T^2$, $\hat{\mu}_0 := \mu_0/\pi T$, and $\hat{\kappa} := \kappa/\pi T$ are the dimensionless quantities.

As R_1 depends on x, we can define the expansion parameter ϵ as the value of $|\langle\mathcal{O}\rangle|$ at $x = l/2$, where $\langle\mathcal{O}\rangle$ is the condensate of the dual field theory defined in the AdS/CFT duality. So, we can normalize

$$\lim_{u\to 0}\rho(u)/u = 1\,, \qquad \zeta(l/2) = 1\,, \quad (15)$$

without loss of generality.

To obtain an analytic solution of Eq. (14), following the procedure of [17], we consider the following particular case:

$$\hat{\kappa}^2 \ll 1, \qquad \lim_{\hat{\kappa}\to 0} \hat{\mu}_0 = 2\,. \tag{16}$$

Expanding Eq. (14) as a series in $\hat{\kappa}^2$, we obtain ρ as

$$\rho = \frac{u}{1+u} - \hat{\kappa}^2 \frac{u\ln(1+u)}{4(1+u)} + O(\hat{\kappa}^4),$$
$$\hat{\mu}_0 = 2 + \frac{1}{2}\hat{\kappa}^2 + O(\hat{\kappa}^4). \tag{17}$$

Integrating Eq. (13) from $x = -\epsilon$ to $x = \epsilon$, we obtain

$$\lim_{\epsilon\to 0}\{\partial_x\zeta(+\epsilon) - \partial_x\zeta(l-\epsilon)\} = g\zeta(0). \tag{18}$$

Then, the general solution of Eq. (13) [1] satisfying Eq. (18) and the normalization (15) is written by

$$\zeta^2 = \frac{1-(v_0/\kappa)^2}{2}\cos 2\kappa(x-l/2) + \frac{1+(v_0/\kappa)^2}{2} \tag{19}$$

with

$$g = \frac{2(1-(v_0/\kappa)^2)\kappa\sin\kappa l}{1+(v_0/\kappa)^2 + (1-(v_0/\kappa)^2)\cos\kappa l}. \tag{20}$$

For given $v_0\,l$ and $g\,l$, we can find the parameters $\kappa\,l$ that satisfy Eq. (20). As shown in Fig. 1, there are two parameters $\kappa_<$, $\kappa_>$ ($\kappa_< < \kappa_>$) for a given $v_0\,l$ when $g\,l$ is smaller than a critical value $g_c\,l$. The two parameters, however, merge at $g_c\,l$ and then beyond it, there is no solution satisfying Eq. (20). The structure of the solutions is very similar to the one found in [5], implying that the solution with $\kappa_>$ is unstable according to a saddle-node bifurcation theory.

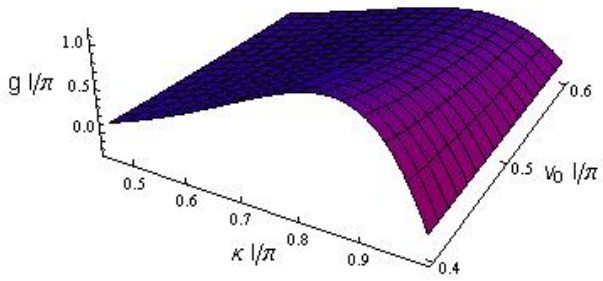

FIG. 1: (color online). The plot of $g\,l$ as a function of $\kappa\,l$ and $v_0\,l$. When v_0 is constant, there are two solutions for κ as far as g is less than a critical value g_c.

[1] In general, there is another solution such that ζ^2 has a local minimum at $x = l/2$. However, this solution must oscillate at least once, so it takes larger value of κ than the one of the solution (19). This implies that it takes more energy than the solution (19).

IV. HIGHER ORDER SOLUTIONS AND THE FREE ENERGY

In this section we construct higher order solutions of Eqs. (11) and show that the solution with larger κ is unstable by calculating the free energy.

A. The construction of $O(\epsilon)$ solutions

At $O(\epsilon)$, the equations of motion are derived from Maxwell Eqs. (9). From the condition (10) and the expansion (11), it follows that the r. h. s. of the x-component of Eqs. (9) is x-independent at $O(\epsilon)$. This implies that $M_x^{(1)}$ is also x-independent. Making the ansatz $M_x^{(1)} = M_x^{(1)}(u)$ and $M_u^{(1)} = 0$, Eqs. (9) are reduced to

$$(1-u^2)M_x^{\prime\prime(1)} - 2uM_x^{\prime(1)} = \frac{v_0\rho^2}{2u^2}\,. \tag{21}$$

From the boundary condition (10) and $\xi(l/2) = v_0$, the asymptotic boundary condition for $M_x^{(1)}$ should be $M_x^{(1)}(0) = 0$. Imposing the regularity condition at the horizon $u = 1$, we obtain the solution, up to $O(\hat{\kappa}^2)$,

$$M_x^{(1)} = \frac{v_0}{32(1+u)}\Bigg[8(1-\hat{\kappa}^2) + \hat{\kappa}^2\{(2\ln 2)(1+u)\ln(1-u)$$
$$- \ln(1+u)(4 + 2(1+u)\ln(1-u) - (1+u)\ln(1+u))\}$$
$$- 2\hat{\kappa}^2(1+u)\mathrm{Li}_2\left(\frac{1+u}{2}\right)\Bigg] - \frac{v_0}{192}\{48 - \hat{\kappa}^2(48+\pi^2 - 6(\ln 2)^2\}$$
$$+ O(\hat{\kappa}^4)\,, \tag{22}$$

where Li_2 is the Polygamma function [21]. The superfluid current $\langle J_x\rangle$ is read off from the derivative of $M_x^{(1)}$ as

$$\langle J_x\rangle \sim M_x^{\prime(1)}(0) = -\frac{v_0}{8}(2 - \hat{\kappa}^2(1-\ln 2))\,. \tag{23}$$

The equation of motion for $M_t^{(1)}$ is given by

$$4u\,\partial_u^2 M_t^{(1)} + \frac{\partial_x^2 M_t^{(1)}}{1-u^2} = \frac{2\mu_0}{u(1+u)}\rho^2\zeta^2$$
$$= \frac{\mu_0\,\rho^2}{u(1+u)}\{(1-\nu^2)\cos 2\kappa(x-l/2) + 1 + \nu^2\}\,, \tag{24}$$

where here and hereafter we set $\nu = v_0/\kappa$ for brevity. Making the ansatz, $M_t^{(1)}(u,x) = \eta_{t0}(u) +$

$\eta_{t1}(u)\cos 2\kappa(x-l/2)$ and imposing the asymptotic boundary condition $\eta_{t1}(0)=0$ by Eq. (10), and the regularity conditions at the horizon, $\eta_{t0}(1)=\eta_{t1}(1)=0$, we obtain

$$\frac{\eta_{t0}}{\pi T} = -C(1-u) + \frac{(1+\nu^2)(1-u)}{8(1+u)} + \frac{\hat{\kappa}^2(1+\nu^2)\{u-1+(1+u)\ln 2 - 2\ln(1+u)\}}{16(1+u)} + O(\hat{\kappa}^4)\,, \tag{25}$$

$$\frac{\eta_{t1}}{\pi T} = -\frac{(1-\nu^2)u(1-u)}{8(1+u)} + \frac{\hat{\kappa}^2(1-\nu^2)u}{16(1+u)}\{1-u-(1+u)\ln 2 + 2\ln(1+u)\} + O(\hat{\kappa}^4)\,, \tag{26}$$

where C is an integration constant determined later.

B. The free energy

To regulate the action (1), we need a counter term $S_{\rm ct}$ defined by

$$S_{\rm ct} := \int d^4x\ \sqrt{-h}\ \left\{ \frac{2\,|\psi|^2}{L} + n^\mu\,\nabla_\mu|\psi|^2 \right\}, \tag{27}$$

where n^μ is defined first as a unit outward normal vector to a $u=const.$ hypersurface with the induced metric h_{ab}, and where the limit $u\to 0$ is taken [17]. Evaluating the action (1) on the onshell condition by using the equation of motion (3) and using the asymptotic form of ψ (6), we find

$$S_{\rm os} = L^3(\pi T)^4 \int d^4x(-2|\beta|^2\ln u + \alpha\beta^* + \alpha^*\beta) - \frac{L^2}{4}\int d^5x\sqrt{-g}F^2. \tag{28}$$

Since we impose $\beta=0$ for the asymptotic boundary condition of ψ, the first term disappears, and there is no contribution from the scalar field.

Using the Maxwell equation $\nabla_\nu F^{\nu\mu}_{(0)}=0$, we find

$$S_{\rm os} = -L^2\int d^4x\sqrt{-h}n^\mu F^{(0)}_{\mu\nu}(M^\nu_{(0)}/2 + \epsilon M^\nu_{(1)} + \cdots) - \frac{\epsilon^2L^2}{2}\int d^4x\sqrt{-h}n^\mu F^{(1)}_{\mu\nu}M^\nu_{(1)} + \frac{\epsilon^2L^2}{2}\int d^5x\sqrt{-g}M^\nu_{(1)}\nabla^\mu F^{(1)}_{\mu\nu} + \cdots\,. \tag{29}$$

As shown in [22], the last term becomes zero under the asymptotic boundary condition $\beta=0$. Then, the free energy $\Omega = -S_{\rm os}/\int dt$ becomes

$$\Omega = 2\pi^2L^3T^2\int d^3x M_t'^{(0)}M_t - \pi^2L^3T^2\int d^3x M_t'^{(0)}M_t^{(0)} + \epsilon^2\pi^2L^3T^2\int d^3x M_t'^{(1)}M_t^{(1)} + \cdots\,. \tag{30}$$

Here, we have used the fact that $M_x'^{(0)}=0$ and $M_x^{(1)}(u=0)=0$.

In the limit $\hat{\kappa}\to 0$ ($T\to\infty$), $M^{(0)}$ is independent of the scalar field configuration of ψ. Furthermore, our asymptotic condition $\mu = M_t(0,x)$ given by Eq. (10) implies that the difference of the free energy between the two solutions with $\kappa_<$ and $\kappa_>$ appears at the last term in Eq. (30), up to $O(\epsilon^2)$. Substitution of the solution (25) and (26) into Eq. (30) yields

$$\Omega = -\epsilon^2\pi^4L^3T^4l\int dydz\times\Gamma,$$
$$\Gamma := \left(C - \frac{1+\nu^2}{8}\right)\left(C - \frac{1+\nu^2}{4} - \frac{(1-\nu^2)\sin\kappa l}{8\kappa l}\right). \tag{31}$$

The constant C is determined by the "orthogonality" condition [2]

$$\int d^5x\sqrt{-g}M^\nu_{(1)}\nabla^\mu F^{(1)}_{\mu\nu} = \int d^5x\sqrt{-g}M^\nu_{(1)}M^{(0)}_\nu R_1^2 = 0, \tag{32}$$

where we used the Maxwell equation (9) in the last line. Substituting Eqs. (22), (25), and (26) into the condition, we find

$$\left[\frac{(1+\nu^2)\sin\kappa l}{2\kappa l} + \frac{1-\nu^2}{4} + \frac{(1-\nu^2)\sin 2\kappa l}{8\kappa l}\right]z_1 + \left[\frac{(1-\nu^2)\sin\kappa l}{2\kappa l} + \frac{1}{2}(1+\nu^2)\right]z_0 + O(\hat{\kappa}^2) = 0 \tag{33}$$

with the coefficients z_0 and z_1 given by

$$z_0 = \frac{1}{192}(5+5\nu^2-48C) + O(\hat{\kappa}^2),$$
$$z_1 = -\frac{1}{192}(1-\nu^2) + O(\hat{\kappa}^2). \tag{34}$$

The chemical potential can be expanded as

$$\hat{\mu} = \frac{M_t(0,x)}{\pi T} = 2 + \frac{\hat{\kappa}^2}{2} + \epsilon\hat{\mu}_1 + \cdots\,,$$
$$\hat{\mu}_1 := -C + \frac{1+\nu^2}{8}. \tag{35}$$

As μ and T are fixed for the two solutions κ_a ($a=>,<$), the expansion parameter ϵ depends on κ_a. We evaluate the free energy (31) in the case of the high temperature limit $\hat{\kappa}\to 0$ and $\epsilon^{1/2}\ll 1$. In this case, substituting Eq. (35) into Eq. (31) and eliminating ϵ, we find

$$\Omega \simeq -(\hat{\mu}-2)^2\pi^4L^3T^4l\int dydz\,\frac{\Gamma}{\hat{\mu}_1^2}\,. \tag{36}$$

This implies that the difference in the free energy between the two solutions is determined by the coefficient $\Gamma/\hat{\mu}_1^2$.

---

[2] For the derivation, see the Appendix A in Ref. [22]

We numerically solve Eq. (33) and find the coefficient $\Gamma/\hat{\mu}_1^2$ for several cases. It turns out that the smaller value κ takes, the larger positive value the coefficient $\Gamma/\hat{\mu}_1^2$ becomes. This indicates that the free energy with the smaller κ ($\kappa_<$) is smaller than the one with the larger κ ($\kappa_>$), as expected. In the $g\,l = 0.6\pi$, $v_0\,l = 0.4\pi$ case, for example, $\kappa_< l = 0.633\,\pi$, $\kappa_> l = 0.957\,\pi$, and $\Gamma/\hat{\mu}_1^2 = 6.854$, $\Gamma/\hat{\mu}_1^2 = 5.917$, respectively.

V. IMPURITY AND THE SPECTRAL FUNCTION

So far, we have discussed properties of our holographic superfluid solutions with taking into account the effects of the background fluid flow v_0. In this section, we turn our attention to the effects of the impurity introduced by the repulsive potential.

According to the dictionary of the AdS/CFT duality, the spectral function is derived from linear perturbation of the background solution obtained in Sec. III and IV. In general, the perturbed variables $\delta\psi$, δA_μ of the scalar field and the gauge field are coupled to each other. However, since the coupling constant is proportional to $\epsilon^{1/2}$ (see, for example, [20]), by taking the limit $\epsilon \to 0$, one can decouple those perturbation variables. Furthermore, by doing so, one can neglect the effects of the background flow v_0 on perturbations, and thereby manifest the effects of the impurity on the spectral function. In what follows, we consider, in this limit $\epsilon \to 0$, the fluctuations of the scalar field with the temperature T and the coupling constant g fixed, while the chemical potential μ taking various different values.

Under the fixed gauge potential $A_\mu = \mu(1-u)\delta_{t\mu}$, the perturbed equation is simply given by Eq. (3). Here, note that the fluctuations of the superfluid velocity is encoded in the phase φ of the perturbed scalar field $\delta\psi$ [3].

Our background solution is independent of t and homogeneous along the direction of $\vec{Y} = (y, z)$, while it is inhomogeneous along the x-direction. In this case, the linear perturbation of the source term $\delta J = e^{-i\omega t + i\vec{q}\cdot\vec{Y}}\delta J(\omega, \vec{q}\,|\,x)$ and the linear response of the condensates $\delta\langle\mathcal{O}\rangle = e^{-i\omega t + i\vec{q}\cdot\vec{Y}}\delta\langle\mathcal{O}(\omega,\vec{q}\,|\,x)\rangle$ are related to each other, via the retarded response function $\mathcal{G}(\omega, \vec{q}\,|\,x, x')$, as follows:

$$\delta\langle\mathcal{O}(\omega,\vec{q}\,|\,x)\rangle = -\int dx'\ \mathcal{G}(\omega,\vec{q}\,|\,x,x')\ \delta J(\omega,\vec{q}\,|\,x')\ . \tag{37}$$

Since the spectral function

$$\rho(\omega,\vec{q}\,|\,x,x') := -\Im\big[\ \mathcal{G}(\omega,\vec{q}\,|\,x,x')\ \big]\ , \tag{38}$$

specifies $\mathcal{G}$ via its spectral representation, let us study the behavior of the spectral function ρ. In order to see the effects of the impurity, we focus on the linear perturbations $\vec{q} = \vec{0}$ which are homogeneous along $\vec{Y} = (y, z)$. (Hereafter we shall omit the argument $\vec{q}$, for simplicity.)

In the evaluation of $\mathcal{G}(\omega\,|\,x, x')$, it is convenient to introduce an appropriate complete orthonormal system (CONS) $\{\chi_j\}$ in the $L^2(\mathbb{R})$ space along the x direction. Then, Eq. (37) is expressed as

$$\delta\langle\mathcal{O}_i(\omega)\rangle = -\sum_j \mathcal{G}_{ij}(\omega)\ \delta J_j(\omega)\ , \tag{39}$$

where

$$\delta J_j(\omega) := \int dx\ \chi_j^*(x)\ \delta J(\omega\,|\,x)\ , \tag{40a}$$

$$\mathcal{G}_{ij}(\omega) := \int dx\,dx'\ \chi_i^*(x)\ \mathcal{G}(\omega\,|\,x,x')\ \chi_j(x')\ , \tag{40b}$$

$$\mathcal{G}(\omega\,|\,x,x') = \sum_{i,j}\chi_i(x)\ \mathcal{G}_{ij}(\omega)\ \chi_j^*(x')\ . \tag{40c}$$

Now let us derive Eq. (39) by using *holographic method*. We seek for a solution of the perturbed scalar field $\delta\psi$ in the form of separation of variables $\delta\psi = e^{-i\omega t}\,U(u)\,X(x)$. The equation of motion for $\delta\psi$ becomes the following set of equations:

$$\left[-\frac{d^2}{dx^2} + g\sum_{n=-\infty}^{\infty}\delta(x-nl)\right]X = \kappa^2\,X\ , \tag{41a}$$

$$\left[\frac{d}{du}\frac{f(u)}{u}\frac{d}{du} + \frac{\{\hat{\omega}+\hat{\mu}(1-u)\}^2}{4u^2 f(u)} + \frac{4-\hat{\kappa}^2 u}{4u^3}\right]U = 0\ , \tag{41b}$$

where $\hat{\omega} := \omega/\pi T$, $\hat{\mu} := \mu/\pi T$, and $\kappa > 0$.

In the limit $\epsilon \to 0$, the background solution in previous sections affects Eq. (41b) only through $\hat{\mu}$. Note that Eq. (41b) is equivalent to Eq. (14) when $\hat{\omega} = 0$.

Let us first analyze Eq. (41a). Since Eq. (41a) corresponds to an energy eigenvalue problem of the Kronig-Penney model consisting of δ-function barriers with certain period, it should admit, as a solution, Bloch states

$$X_k(x+l) = e^{ikl}\,X_k(x) \qquad (-\infty < k < \infty)\ . \tag{42}$$

Demanding the orthonormal condition,

$$\int_{-\infty}^{\infty} dx\ X_k^*(x)\,X_{k'}(x) = \delta(k-k')\ , \tag{43}$$

we find the solutions to Eqs. (41a) and (42) as

$$X_k(0<x<l) = \{8\pi\,\sin\kappa\,l\ \sin k\,l\ (dk/d\kappa)\}^{-1/2} \times\left\{\left(e^{ikl}-e^{-i\kappa l}\right)e^{i\kappa x} - \left(e^{ikl}-e^{i\kappa l}\right)e^{-i\kappa x}\right\}\ . \tag{44}$$

Here κ is a positive definite function $\kappa(k) > 0$ of the wave number k and is determined by [23],

$$-1 \le \cos k\ell = \cos\kappa\ell + \frac{g\,\ell}{2}\,\frac{\sin\kappa\ell}{\kappa\ell} \le 1\ . \tag{45}$$

[3] The velocity corresponds to the derivative of φ with respect to x.

Note that $\kappa(k) = \kappa(-k)$, $X_k^*(x) = X_{-k}(x)$.

The condition (45) places a restriction on the range of κ for a given g, yielding a band structure shown in Fig. 2. The shaded region represents the allowed region satisfying Eq. (45), while the blank region corresponds to the forbidden region. Let us denote by κ_n the bottom of the n-th allowed band. Then, the first and the second allowed bands are given respectively by $\kappa_1 < \kappa < \pi/l$ and $\kappa_2 < \kappa < 2\pi/l$. For $g\,l = 0.663\,\pi$, $\kappa_1\,l = 0.423\,\pi$, $\kappa_2\,l = 1.175\,\pi$.

In the case of $v_0\,l = \pi/2$, the dot-dashed (blue) curve represents the function g of κ given by Eq. (20), while the dashed (black) and solid (green) curves represent the ones with $v_0\,l = 0.421\,\pi$ and $v_0\,l = 0.225\,\pi$, respectively.

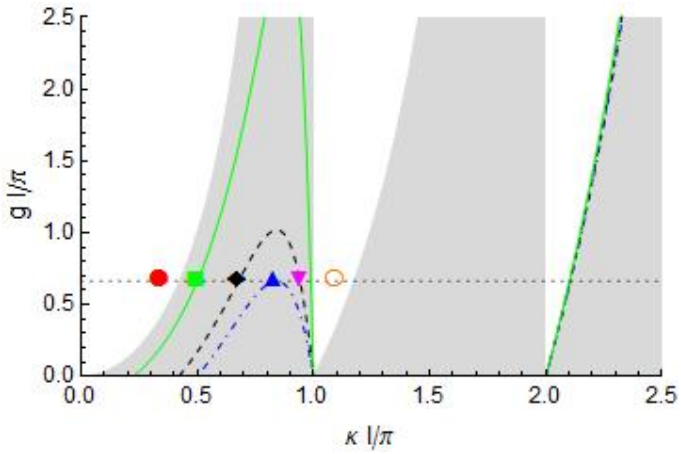

FIG. 2: (color online). The band structure given by the repulsive potential (5). The shaded region is the allowed region in which Eq. (45) holds, and the blank region is forbidden one. The dot-dashed (blue) curve represents the function g given by Eq. (20) with $v_0\,l = \pi/2$, while the dashed (black) and solid (green) curves represent the ones with $v_0\,l = 0.421\,\pi$ and $v_0\,l = 0.225\,\pi$, respectively. The horizontal black dotted line expresses the local maximum value ($g\,l = 0.663\,\pi$) of the blue dot-dashed curve. The six points on the horizontal dotted line correspond to $\kappa_* l/\pi := Tl\,\hat{\kappa}_*(\hat{\mu})$ for the value of the chemical potential $\mu l/\pi$ respectively, 2.060 (●, red), 2.120 (■, green), 2.215 (◆, black), 2.321 (▲, blue), 2.400 (▼, magenta), 2.519 (○, orange) when $Tl = 1$ and $g\,l = 0.663\,\pi$.

Let us turn to Eq. (41b). Hereafter, by U_k we denote U that couples to X_k[4] so that $\delta\psi \propto X_k\,U_k$. Near the AdS boundary $u \sim 0$, it becomes

$$\left(\frac{d}{du}\,\frac{1}{u}\,\frac{d}{du} + \frac{1}{u^3}\right) U_k \sim 0\ , \tag{47}$$

and therefore its solution behaves asymptotically as

$$U_k(u) \sim -\alpha(\hat{\kappa}(k), \hat{\mu}, \hat{\omega})\,u + \beta(\hat{\kappa}(k), \hat{\mu}, \hat{\omega})\,u \ln u\ . \tag{48}$$

Here we have taken into consideration the fact that the wave number k contributes to the above formula only through $\hat{\kappa}(k)$ in Eq. (41b).

Note that α and β are related in a certain manner so that at the horizon $u \to 1$, U_k satisfies the ingoing boundary conditions. This, together with the fact that Eq. (41b) with different wave number k is independent of each other, implies that the expectation value $\alpha(\hat{\kappa}(k))$ couples only to the source $\beta(\hat{\kappa}(k))$ with the same wave number k. Therefore we can diagonalize $\mathcal{G}_{ij}(\omega)$ in Eq. (39) so that $\mathcal{G}_{kk'}(\hat{\omega}) = \mathcal{G}_{\hat{\kappa}}(\hat{\omega})\,\delta(k-k')$, with $\mathcal{G}_{\hat{\kappa}}(\hat{\omega})$ given below. Note that $\mathcal{G}_{\hat{\kappa}}(\hat{\omega})$ is labeled only by $\hat{\kappa}$, since α and β has a dependency on k only through $\hat{\kappa}$. Thus, we obtain the retarded response function as

$$\begin{aligned}\mathcal{G}(\hat{\omega}\,|\,x, x') &= \int_{-\infty}^{\infty} dk\ \mathcal{G}_{\hat{\kappa}}(\hat{\omega})\,X_k(x)\,X_k^*(x') \\ &= 2\int_0^{\infty} dk\ \mathcal{G}_{\hat{\kappa}}(\hat{\omega})\,\Re\left[\,X_k(x)\,X_k^*(x')\,\right]\ , \end{aligned} \tag{49a}$$

$$\mathcal{G}_{\hat{\kappa}}(\hat{\omega}) := -\frac{\alpha(\hat{\kappa}(k), \hat{\mu}, \hat{\omega})}{\beta(\hat{\kappa}(k), \hat{\mu}, \hat{\omega})}\ . \tag{49b}$$

The behavior of the retarded response function $\mathcal{G}_{\hat{\kappa}}(t)$ with real time t is determined by the singularity structure of $\mathcal{G}_{\hat{\kappa}}(\hat{\omega})$ with respect to the complex $\hat{\omega}$. We can find the relaxation time scale of the condensate by inspecting quasinormal (QN) frequency $\hat{\omega} = \hat{\Omega}_{\rm QNM}(\hat{\kappa}, \hat{\mu})$, which is a solution to $\beta(\hat{\kappa}, \hat{\mu}, \hat{\omega}) = 0$ and provides the poles of $\mathcal{G}_{\hat{\kappa}}(\hat{\omega})$. Furthermore, we find a critical point from either the highest value of $\hat{\mu}$ ($\hat{\mu} = \hat{\mu}_*(\hat{\kappa})$) or the lowest value of $\hat{\kappa}$ ($\hat{\kappa} = \hat{\kappa}_*(\hat{\mu})$) that solves the source free condition for linear perturbation (response) field in the stationary case. As shown later, the spectral function crucially depends on the background parameter $\hat{\kappa}_*(\hat{\mu})$.

Now let us see the behavior of the spectral function at the point $x = x' = l/2$, avoiding in particular the location of the impurity itself. Define $\rho(\hat{\omega}) := \rho(\hat{\omega}\,|\,l/2, l/2)$. Then from Eqs. (38), (44), and (49a), we obtain:

$$\rho(\hat{\omega}) = -\int_{\mathcal{B}} \frac{d\kappa}{\pi}\,\Im\left[\,\mathcal{G}_{\hat{\kappa}}(\hat{\omega})\,\right]\,\mathcal{W}(\kappa\,l,\, g\,l)\ , \tag{50a}$$

$$\mathcal{W}(\sigma,\, g\,l) := \frac{\sin\sigma + (g\,l/2\,\sigma)\,(1-\cos\sigma)}{\sin k\,l} \tag{50b}$$

$$= \sqrt{\frac{2\,\sigma + g\,l\,\tan(\sigma/2)}{2\,\sigma - g\,l\,\cot(\sigma/2)}}\ , \tag{50c}$$

where the domain of integration $\mathcal{B}$ satisfies Eq. (45) with $\kappa > 0$ and is determined by $g\,l$. We list below the basic properties of the spectral function $\rho(\hat{\omega})\,l$, obtained by inspecting Eq. (50):

- The spectral function $\rho(\hat{\omega})\,l$ is specified by $\hat{\mu}$, $T\,l$, and $g\,l$. (Note that $\hat{\kappa} = \kappa\,l/(\pi\,T\,l)$).

[4] Note that in what follows, we assume that the orthonormal Bloch states (44) form a CONS on the $L^2(\mathbb{R})$ space defined by

$$\int_{-\infty}^{\infty} dk\ X_k(x)\,X_k^*(x') = \delta(x-x')\ . \tag{46}$$

- The dependency on $\hat{\mu}$ and $T\,l$ is determined by $\mathcal{G}_{\hat{\kappa}}(\hat{\omega})$. Eq. (41b), which provides $\mathcal{G}_{\hat{\kappa}}(\hat{\omega})$, is the same as the equation for linear perturbations with wave number k on the homogeneous background field with no impurity. (To see this, replace $\hat{\kappa}$ with $k/\pi T$.) From the dependency of $\mathcal{G}_{\hat{\kappa}}(\hat{\omega})$ on low-$\hat{\omega}$ and $\hat{\kappa}$ around the critical point $\hat{\mu} \lesssim \hat{\mu}_*(\hat{\kappa})$, it turns out that our holographic superconductor exhibits the critical dynamics of model A [24]. (See Ref [25] for a review of dynamic critical phenomena, and also [26] for the introduction of dynamic critical phenomena. The study of dynamic critical phenomena in the AdS/CFT context is given by, e.g., [27–29].)

- The effects of the impurity appear via the band structure $\mathcal{B}$ and the weight $\mathcal{W}(\kappa\,l,\, g\,l)$.

- Due to "$\sin k\,l$" in the denominator of Eq. (50b) (or Eq. (50c)), the weight $\mathcal{W}$ diverges at the edge of the band, where $\cos k\,l = \pm 1$. Since $1/\sin k\,l \propto dk/d\kappa$ from Eq. (45), the divergence of $\mathcal{W}$ is related to that of the state density per unit "energy" $E := \kappa^2$, i.e., dk/dE. This is a reminiscent of the fact that in superfluid, local dynamical response function exhibits a singular behavior around the critical velocity[30, 31]. The divergence of state density at the critical velocity is the origin of the singular behavior.

In Fig. 3, we plot the spectral function at $x = l/2$, $\rho(\hat{\omega})$, for various chemical potentials μ for $T\,l = 1$ and $g\,l = 0.663\,\pi$ case. Then, the behavior of the spectral function is qualitatively determined by the position of $\kappa_* := \pi T\,\hat{\kappa}_*$. When $\kappa_*\,l/\pi = (T\,l)\,\hat{\kappa}_*$ is in the blank region in Fig. 2, the spectral function rapidly increases as $\hat{\omega}$ increases (see the red ($\kappa_*\,l = 0.35\,\pi$) and orange curve ($\kappa_*\,l = 1.1\,\pi$) in Fig. 3). On the other hand, when $\kappa_*\,l/\pi$ is in the gray region in Fig. 2, the spectral function does not change rapidly in the low frequency region, and it decays around $\hat{\omega} \sim 0.1$ (see the other curves in Fig. 3).

The behavior of $\rho(\hat{\omega})$ shown in Fig. 3 can be explained by inspecting the dependency of $\rho_{\hat{\kappa}}(\hat{\omega}) := -\Im[\,\mathcal{G}_{\hat{\kappa}}(\hat{\omega})\,]$ on $\hat{\mu}$ (or $\hat{\kappa}_*$) and κ, and by taking the existence of a band gap into consideration.

We first note that $\mathcal{G}_{\hat{\kappa}}(\hat{\omega})$ is expressed in terms of its QN frequencies $\{\hat{\Omega}_{\mathrm{QNM},j}\}_{j=0,1,2,\cdots}$ as

$$\mathcal{G}_{\hat{\kappa}}(\hat{\omega}) = \sum_j \frac{a_j(\hat{\kappa},\hat{\mu})}{\hat{\omega} - \hat{\Omega}_{\mathrm{QNM},j}(\hat{\kappa},\hat{\mu})} + \cdots\ ,$$

where a_j denotes the residues of $\mathcal{G}_{\hat{\kappa}}(\hat{\omega})$ at $\hat{\omega} = \hat{\Omega}_{\mathrm{QNM},j}$. Now, let $\hat{\boldsymbol{\Omega}}(\hat{\kappa},\hat{\mu})$ be the QN frequencies whose imaginary parts take the smallest in their absolute value. From the above expression of $\mathcal{G}_{\hat{\kappa}}(\hat{\omega})$, we find that for real $\hat{\omega}$, such an $\hat{\boldsymbol{\Omega}}(\hat{\kappa},\hat{\mu})$ can contribute most to $\mathcal{G}_{\hat{\kappa}}(\hat{\omega})$, hence to $\rho_{\hat{\kappa}}(\hat{\omega})$,

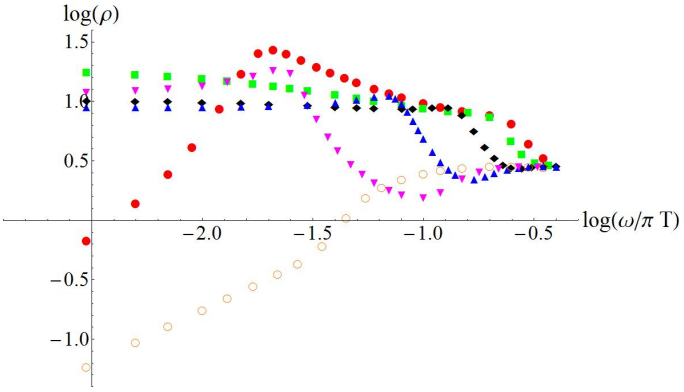

FIG. 3: (color online). The Log-Log plot of the spectral function $\rho(\hat{\omega})$ is shown for various chemical potentials $\mu\,l/\pi$ (2.060 (●, red), 2.120 (■, green), 2.215 (◆, black), 2.321 (▲, blue), 2.400 (▼, magenta), 2.519 (○, orange) when $Tl = 1$ and $g\,l = 0.663\,\pi$. Note that these points with the colors (red, green, black, blue, magenta, and orange) correspond respectively to the points on the horizontal black dotted line with the same colors in Fig. 2

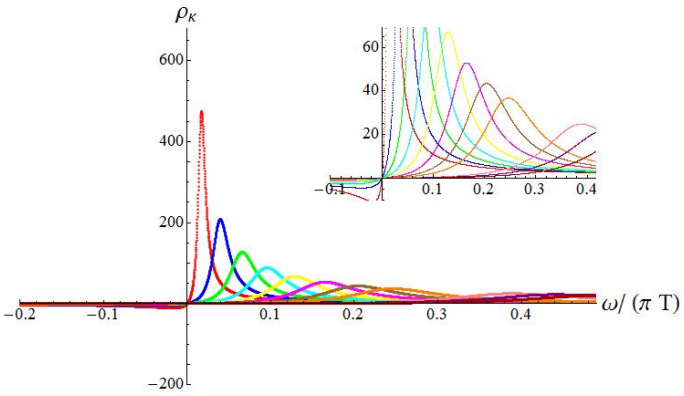

FIG. 4: (color online). Plots of $\rho_{\hat{\kappa}}(\hat{\omega})$ for various different values of $\hat{\kappa}$ with $\hat{\kappa}_* = 0.35$, corresponding to the red plot (●) in Fig.3 The location of peak shifts to the right, as $\hat{\kappa}$ increases from $\hat{\kappa} = 0.423$ with the difference $\Delta\hat{\kappa} = 0.08$ between every adjacent two peaks. When $T\,l = 1$, $\hat{\kappa} \simeq 0.423$, which gives the peak closest to the origin, corresponds to, $\kappa_1 l/\pi \sim 0.423$, the bottom of the first allowed band for $g\,l = 0.663\,\pi$. One can find the disappearance of peaks around $\hat{\omega} = 0.32$ due to the band gap for $\hat{\kappa} = 1.063$ and 1.143.

and we have

$$\mathcal{G}_{\hat{\kappa}}(\hat{\omega}) \sim \frac{\boldsymbol{a}(\hat{\kappa},\hat{\mu})}{\hat{\omega} - \hat{\boldsymbol{\Omega}}(\hat{\kappa},\hat{\mu})} = \frac{\boldsymbol{a}\,(\hat{\omega} - \hat{\boldsymbol{\Omega}}^*)}{|\,\hat{\omega} - \hat{\boldsymbol{\Omega}}\,|^2}\ .$$

Then, the behavior of $\rho_{\hat{\kappa}}(\hat{\omega})$ can be understood in terms of $\hat{\boldsymbol{\Omega}}(\hat{\kappa},\hat{\mu})$ via the following formula:

$$\rho_{\hat{\kappa}}(\hat{\omega}) \sim -\frac{\Im(\boldsymbol{a})\ \hat{\omega}}{|\,\hat{\omega} - \hat{\boldsymbol{\Omega}}(\hat{\kappa},\hat{\mu})\,|^2}\ , \tag{51}$$

where we have set $\Im[\,\boldsymbol{a}\,\hat{\boldsymbol{\Omega}}^*\,] = 0$ as $\rho_{\hat{\kappa}}(\hat{\omega} = 0) = 0$.

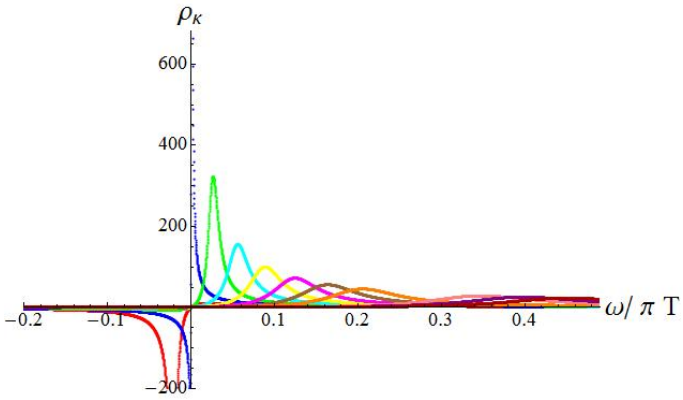

FIG. 5: (color online). Plots of $\rho_{\hat{\kappa}}(\hat{\omega})$ for various different values of $\hat{\kappa}$ with $\hat{\kappa}_* = 0.50$, corresponding to the green plot (■) in Fig.3. The plots with the same color in this figure and Fig. 4 are for the same values of $\hat{\kappa}$. Due to the large value of $\hat{\kappa}_*$ (or $\hat{\mu}$) than that for Fig. 4, every peak is shifted to the left compared to the location of the corresponding peak in Fig. 4. The disappearance of peaks due to the band gap is also shifted to around $\hat{\omega} = 0.29$. Note also that there is a mode that has a peak arbitrarily close to $\omega = 0$, as $0.423 < \hat{\kappa}_*$.

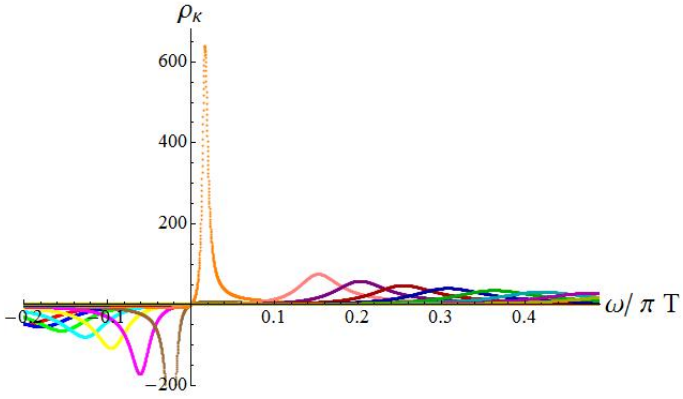

FIG. 6: (color online). Plots of $\rho_{\hat{\kappa}}(\hat{\omega})$ for various different values of $\hat{\kappa}$ with $\hat{\kappa}_* = 0.95$, corresponding to the magenta plot (▼) in Fig.3. The location of every peak is shifted further to the left, and the disappearance of peaks due to the band gap is now around $\hat{\omega} = 0.06$, which forms the slope around $\log(\omega/\pi T) = -1.25$ in Fig.3.

We find that $\hat{\mathbf{\Omega}}(\hat{\kappa}, \hat{\mu})$ has the following properties:

- When $\hat{\kappa} = \hat{\kappa}_*(\hat{\mu})$, $\hat{\mathbf{\Omega}} = 0$[5], and when $\hat{\kappa} \gtrless \hat{\kappa}_*(\hat{\mu})$, $\Im[\,\hat{\mathbf{\Omega}}(\hat{\kappa}, \hat{\mu})\,] \lesseqgtr 0$. That is, perturbations with $\hat{\kappa} > \hat{\kappa}_*(\hat{\mu})$ are stable ones, while those with $\hat{\kappa} < \hat{\kappa}_*(\hat{\mu})$ are unstable ones.

[5] This is indicated from the fact that $\hat{\mu}_*$ ($\hat{\kappa}_*$) satisfies the source free condition of Eq. (41b) with $\hat{\omega} = 0$ (i.e., boundary conditions at the infinity for QN frequencies). For $\hat{\kappa} = 0$, such a massless mode may be viewed as the emergence of a holographic Nambu-Goldstone mode in the condensation phase [32].

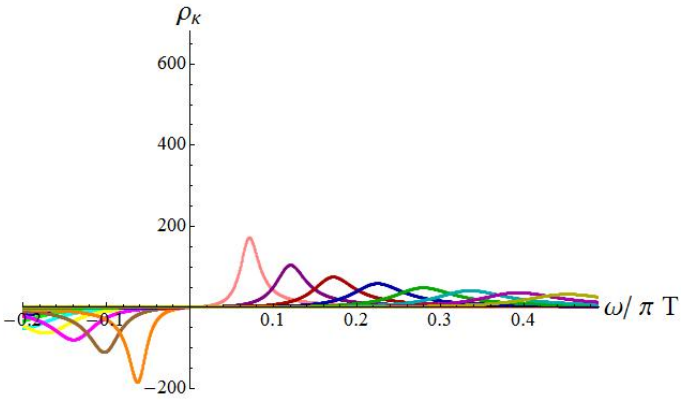

FIG. 7: (color online). Plots of $\rho_{\hat{\kappa}}(\hat{\omega})$ for various different values of $\hat{\kappa}$ with $\hat{\kappa}_* = 1.10$, corresponding to the magenta plot (○) in Fig.3. The disappearance of peaks due to the band gap is now around $\hat{\omega} \sim 0$, and $\rho(\hat{\omega} \sim 0^+)$ takes vanishingly small values, corresponding to the behavior of the orange plot in Fig.3.

- Since $\hat{\kappa}_*(\hat{\mu})$ is an increasing function, as $\hat{\mu}$ increases, the stable perturbations change to unstable ones, and at the marginal limit $\hat{\mu} \nearrow \hat{\mu}_*(\hat{\kappa})$ ($\hat{\kappa}_*(\hat{\mu}) \nearrow \hat{\kappa}$), $\hat{\mathbf{\Omega}} \to 0$ [24, 32]. This implies that $\hat{\mathbf{\Omega}}$ is continuous with $\hat{\mu}$.

- For the stable perturbations with $\hat{\kappa} > \hat{\kappa}_*(\hat{\mu})$, both the magnitude of the real part of $\hat{\mathbf{\Omega}}(\hat{\kappa}, \hat{\mu})$ and that of the imaginary part are increasing functions with respect to $\hat{\kappa}$.

From the observations above, we can expect $\rho_{\hat{\kappa}}(\hat{\omega})$ to behave as follows:

- As Eq. (51) shows, $\rho_{\hat{\kappa}}(\hat{\omega})$ possesses a Lorentzian peak of width about $|\Im[\,\hat{\mathbf{\Omega}}(\hat{\kappa}, \hat{\mu})\,]|$ at $\hat{\omega} = \Re[\,\hat{\mathbf{\Omega}}(\hat{\kappa}, \hat{\mu})\,]$. (In what follows we assume $\Re(\hat{\mathbf{\Omega}}) > 0$.)

- As the marginal limit $\hat{\mu} \nearrow \hat{\mu}_*(\hat{\kappa})$ ($\hat{\kappa}_*(\hat{\mu}) \nearrow \hat{\kappa}$) is approached, the peak of $\rho_{\hat{\kappa}}(\hat{\omega})$ is getting narrow in width and sharp, and its location is approaching $\hat{\omega} = 0$.

- The modes which become unstable beyond the marginal limit possess a negative peak in the range $\hat{\omega} < 0$.

Figs. 4-7 show that our expectations about the behavior of $\rho_{\hat{\kappa}}(\hat{\omega})$ listed above are in fact true.

As in Eq. (50), the local spectral function $\rho(\hat{\omega})$ can be obtained by the (weighted with $\mathcal{W}$) summation of $\rho_{\hat{\kappa}}(\hat{\omega})$. Then, from Figs. 4-7, we can find the behavior of $\rho(\hat{\omega})$ in Fig. 3 as follows:

- $(T\,l)\,\hat{\kappa}_*(\hat{\mu}) < \kappa_1\,l/\pi$ (Fig. 4)

  The minimum value of κ is κ_1, whose peak location, $\hat{\omega}_1 := \Re[\,\hat{\mathbf{\Omega}}(\kappa_1/\pi T, \hat{\mu})\,]$, is the closest to $\hat{\omega} = 0$ and

the tallest among others. As $\hat{\kappa}$ increases, the peak is shifted to the right and its shape becomes short in height and wide width. Then, $\rho(\hat{\omega})$ obtained by summing up such short and wide profiles increases with $\hat{\omega}$ in a neighborhood $\hat{\omega} \gtrsim 0$, admits a peak around $\hat{\omega}_1$, and then monotonically decreases as the red plots in Fig.3.

- $\kappa_1\, l/\pi < (T\, l)\, \hat{\kappa}_*(\hat{\mu}) < 1$ (Figs. 5, 6)

  In this case $\hat{\omega}_1 < 0$. Since $\hat{\kappa}_*(\hat{\mu})$ is in the first allowed band, there exists a mode of $\hat{\kappa}$ which can arbitrarily be close to $\hat{\kappa}_*$, and in the range $\hat{\omega} > 0$, sharp peaks continue to $\hat{\omega} = 0$. For this reason, $\rho(\hat{\omega})$ does not show an increasing behavior in $\hat{\omega}$ in a neighborhood of $\hat{\omega} = 0$ shown in Fig. 3.

  Also in that neighborhood, the disappearance of peaks due to the band gap makes $\rho(\hat{\omega})$ decreasing, reflected in the plots on the decreasing slope (with colors, green, black, blue, and magenta) in Fig. 3.

- $1 < (T\, l)\, \hat{\kappa}_*(\hat{\mu}) < \kappa_2\, l/\pi$ (Fig. 7)

  Due to the band gap, there are no peaks in a neighborhood of $\hat{\omega} = 0$; no contribution to $\rho(\hat{\omega})$ in the neighborhood of $\hat{\omega} = 0$. Therefore the region of $\hat{\omega} \gtrsim 0$ looks similar to Fig. 4. As a result, the plot of $\rho(\hat{\omega})$ also becomes similar to that of $(T\, l)\, \hat{\kappa}_*(\hat{\mu}) < \kappa_1\, l/\pi$ (see the red plots in Fig. 4).

Although in this section we focused on the impurity and spectral function with neglecting the effects of the background flow v_0, in order to obtain some insights into critical behavior in our holographic superfluid models, we may give the following interpretation on the relation between κ_* and the background flow v_0.

By Eq. (20), $\kappa_*\, l$ $(= \pi\, T\, l\, \hat{\kappa}_*)$ is related to the background fluid flow velocity $v_0\, l$. Then, the parameter values $\kappa_*\, l/\pi = 0.5$ (green), 0.677 (black), and 0.840 (blue) in Fig. 3 correspond respectively to $v_0\, l/\pi = 0.225$, 0.421, and 0.5.

As explained in Sec. III, there are two solutions κ_* satisfying Eq. (20) when $v_0 < v_c$. In the above case, $v_c\, l \simeq 0.5\, \pi$, so the blue curve in Fig. 3 corresponds to the almost critical case where the two solutions merge.

As v_0 approaches the threshold v_c from below, a small hill accompanied with a steep slope emerges in the spectral function $\rho(\hat{\omega})$ around $\hat{\omega} = \omega/\pi T \sim 0.1$ (blue curve). The divergent state density at the edge of the band gap, $\kappa\, l = \pi$ induces the small hill, while the steep slope is caused by the band gap above, $\kappa\, l > \pi$, as discussed above. Fig. 3 shows that the slope becomes steep as v_0 approaches the threshold v_c from below. This reflects the fact that the imaginary part of the QN frequencies, $\hat{\mathbf{\Omega}}(\hat{\kappa}, \hat{\mu})$ in the band gap, $\kappa l > \pi$ becomes small as κ_* approaches the edge of the band gap, $\kappa l = \pi$.

VI. SUMMARY AND DISCUSSIONS

We have investigated holographic models of one-dimensional superfluid flow solutions in the presence of an external repulsive potential. Our solutions are a generalization of the solution of the GP equation [5] to the strongly coupled case. Our solutions possess the properties very similar to those found in GP equation: (i) There are two solutions below the critical value g_c of the coupling constant g, and they merge at g_c. (ii) The free energy of the solution with steeper configuration is higher than the other solution, implying that the solution with steeper configuration is unstable.

We have also studied the spectral function derived from the perturbation of the steady superfluid flow solution. Due to the band structure generated by the periodic repulsive potential, the qualitative features of the spectral function are essentially determined by the parameter κ_* which satisfies $\beta(\kappa_*, \omega = 0) = 0$. As shown in Fig. 3, as κ_* approaches the edge of the band from the left hand side, a small hill appears. This reflects the fact that the state density, hence $\mathcal{W}$, diverges at the edge.

For the solution of one-dimensional superfluid flow [5], the spectral function $\rho(\omega)$ of the local density fluctuation was derived by solving Bogoliubov equation of the GP equation [30, 31]. Near the saddle-node bifurcation, the characteristic frequency ω^* corresponding to the peak of the spectral function scales as $\omega^* \sim |g - g_c|^{1/2}$. Furthermore, $\rho(\omega)$ behaves as $\rho(\omega < \omega^*) \propto \omega^{\beta_1}$ and $\rho(\omega > \omega^*) \propto \omega^{\beta_2}$, where $\beta_1 - \beta_2 = 2$. This is quite different from the spectral function we obtained. One of the main reasons for this is that we derived the spectral function in the limit $\epsilon \to 0$. In this limit, the perturbed equation does not include the background solution explicitly. To derive such critical phenomena, it would be interesting to calculate the spectral function in the case $\epsilon > 0$, taking into account the fluctuations of the gauge field.

Acknowledgments This work was supported in part by JSPS KAKENHI Grant Number 15K05092(AI), 23740200 (KM), and 23540326(TO).

[1] R. P. Feynman, Chap. 2 in Prog. Low Temp. Phys., Vol. I, ed. by C. J. Gorter (North Holland, 1955).
[2] E. P. Gross, Nuovo Cimento **20**, 454 (1961).
[3] L. P. Pitaevskii, Zh. Eksp. Teor. Fiz. **40**, 646 (1961)
[4] T. Frisch, Y. Pomeau, and S. Rica, Phys. Rev. Lett. **69** 1644 (1992).
[5] V. Hakim, Phys. Rev. **E55** 2835 (1997).
[6] C. Raman et. al., Phys. Rev. Lett. **83** 2502 (1999).
[7] R. Onofrio et. al., Phys. Rev. Lett. **85** 2228 (2000).
[8] S. Inouye et. al., Phys. Rev. Lett. **87** 080402 (2001).
[9] Y. Pomeau and S. Rica, C. R. Acad. Sci. Ser. Gen., Ser. 2 **316**, 1523 (1993).
[10] J. M. Maldacena, Adv. Theor. Math. Phys. **2**, 231 (1998) [Int. J. Theor. Phys. **38**, 1113 (1999)]

[11] S. A. Hartnoll, C. P. Herzog, and G. T. Horowitz, Phys. Rev. Lett. **101** 031601 (2008).

[12] S. A. Hartnoll, C. P. Herzog, and G. T. Horowitz, JHEP **12** 015 (2008).

[13] G. T. Horowitz, Lect. Notes in Physics **828** 313 (2011).

[14] G. T. Horowitz, J. E. Santos, and B. Way, Phys. Rev. Lett. **106** 221601 (2011).

[15] N. Iizuka, A. Ishibashi, and K. Maeda, Phys. Rev. Lett. **113** 011601 (2014).

[16] P. Breitenlohner and D. Z. Freedman, Annals Phys. **144**, 249 (1982).

[17] C. P. Herzog, Phys. Rev. **D81**, 126009 (2010).

[18] F. Bloch, Z. Physik. **52**, 545 (1929).

[19] C. P. Herzog, P. K. Kovtun, and D. T. Son, Phys. Rev. **D79**, 066002 (2009).

[20] K. Maeda and T. Okamura, Phys. Rev. **D78**, 106006 (2008).

[21] Handbook of Mathematical Functions, (Dover, New York, 1965) edited by M. Abramowitz, and I.A. Stegun.

[22] K. Maeda, M. Natsuume, and T. Okamura, Phys. Rev. **D81**, 026002 (2010).

[23] C. Kittel, *Introduction to Solid State Physics* (Wiley, New York, 1976).

[24] K. Maeda, M. Natsuume and T. Okamura, Phys. Rev. D **79**, 126004 (2009).

[25] P. C. Hohenberg and B. I. Halperin, Rev. Mod. Phys. **49** (1977) 436.

[26] J. L. Cardy, *Scaling and renormalization in statistical physics* (Cambridge Univ. Press, 1996); N. Goldenfeld, *Lectures on phase transitions and the renormalization group* (Addison-Wesley, 1992).

[27] K. Maeda, M. Natsuume and T. Okamura, Phys. Rev. D **78**, 106007 (2008).

[28] A. Buchel, Nucl. Phys. B **841**, 59 (2010).

[29] M. Natsuume and T. Okamura, Phys. Rev. D **83**, 046008 (2011).

[30] Y. Kato and S. Watabe, J. Low Temp Phys **158** 92 (2010)

[31] Y. Kato and S. Watabe, Phys. Rev. Lett. **105** 035302 (2010).

[32] I. Amado, M. Kaminski and K. Landsteiner, JHEP **0905**, 021 (2009).